EEET ECOLOGICAL ENGINEERING & ENVIRONMENTAL TECHNOLOGY

Ecological Engineering & Environmental Technology, 2026, 27(8), 408–430
https://doi.org/10.12912/27197050/225543
ISSN 2719–7050, License CC-BY 4.0

Received: 2026.06.26
Accepted: 2026.07.10
Published: 2026.08.01

Groundwater recharge potential mapping using piezometric data, remote sensing, GIS-based algorithms, and machine learning in the Ansegmir River Watershed, Upper Moulouya region, Morocco

Hassan Rahoui[1*], Ayoub Sguigaa[1], Mohamed Sabir[1], Said Chakiri[2], Imane Sebari[3], Allal Labriki[4], Mohamed Sadiki[5]

[1] Department of Forest Development, National School of Forestry Engineers, BP 511 Tabriquet, Salé, Morocco
[2] Scientific Institute, Mohammed V University, P.O. Box 703, Rabat, Morocco
[3] Agronomic and Veterinary Institute Hassan II, Rabat, Morocco
[4] Laboratory of Geosciences, Geomatics, and Environment (L2GE), Faculty of Sciences Ben M'Sik, Hassan II University, P.O. Box 7955, Casablanca, Morocco
[5] Geosciences and Natural Resources Laboratory, Faculty of Science, Ibn Tofail University, P.O. Box 133, Kenitra, Morocco
* Corresponding author's e-mail: hassan.rahoui@uit.ac.ma

ABSTRACT

Groundwater recharge in semi-arid mountainous environments is controlled by complex climatic, geological, topographical and anthropogenic interactions. In the Moroccan Atlas Mountains, snowmelt plays a crucial role in sustaining surface and groundwater resources, which are increasingly threatened by agricultural expansion and climate variability. In this context, the Midelt Aquifer within the Ansegmir River Watershed (ARW) represents a strategic water resource for irrigated agriculture, particularly apple orchards that heavily depend on groundwater extraction. This study aims to map the groundwater recharge potential of the Midelt aquifer (241 km²), in response to the expansion of orchards within the Oued Ansegmir watershed. The study integrates piezometric data, remote sensing (RS), GIS-based algorithms and machine learning (ML) approaches. Three modeling techniques were compared: frequency ratio (FR), Random Forest (RF) and extreme gradient boosting (XGBoost). The models were calibrated using 271 field measured piezometric observations used directly as the target variable (70:30), and 16 conditioning factors retained after a Pearson correlation and variance inflation factor (VIF) analyses. Performance was evaluated on an independent test set (n = 82) using ten complementary metrics, ROC curves, confusion matrices, radar plots, an inter-model agreement matrix, and pixel by pixel spatial consensus analysis. XGBoost outperformed the other two models (AUC = 0.769, F1 = 0.590, Kappa = 0.356) and demonstrated remarkable consistency in the spatial validation, particularly in identifying areas with low recharge potential. Therefore, it was selected to produce the final groundwater recharge potential map. These results provide a scientific basis for sustainable groundwater management and the prioritization of future drilling activities within the ARW.

Keywords: hydrogeology, machine learning, geographic information system, remote sensing, piezometric observations, groundwater recharge potential mapping, Ansegmir River Watershed.

INTRODUCTION

Groundwater recharge originates from multiple sources, including direct infiltration of precipitation, snowmelt, river seepage, and anthropogenic inputs such as irrigation return flows and artificial recharge (Döll and Flörke, 2005; Scanlon et al., 2006). Among these, precipitation remains the primary contributor to aquifer replenishment (Jasechko and Perrone, 2021), while the contribution of snowmelt is particularly significant in mountainous regions, where it controls both surface water and groundwater dynamics (Boudhar et al., 2009; Hanich et al., 2022). The spatial distribution and magnitude of groundwater recharge are strongly influenced by the geological setting and topographic features of the study area, both of which exert a strong control on infiltration pathways and recharge rates (Meng et al., 2024).

Indeed, the contribution of precipitation to groundwater recharge is generally low and spatially localized. In semi-arid environments, with an average annual rainfall of around 560 mm, recharge accounts from approximately 4% to 9% of total precipitation. In contrast, in lacustrine areas receiving about 350 mm/year, this contribution ranges from 0.5% to 0.8% (Leduc et al., 2001).

In the semi-arid Atlas Mountains of Morocco specifically, snowmelt has been shown to contribute between 15% and 51% of streamflow (Hanich et al., 2022; Acharki et al., 2025) and between 30% and 80% of groundwater recharge, with direct recharge occurring in response to winter precipitation and a delayed contribution observed during the summer melting season (Boudhar et al., 2009; Hanich L. et al., 2022; Marchane et al., 2023; Acharki et al., 2025).

However, numerous semi-arid and arid basins subjected to human pressures are characterized by scarce rainfall, elevated evapotranspiration rates, and a significant reduction in groundwater recharge (Pande, 2021). This situation not only intensifies the challenge of meeting water demands but also calls for the adoption of management practices that safeguard groundwater sustainability (El Farchouni et al., 2025).

Given that groundwater recharge potential (GWRP) refers to the ability of a hydrogeological system to facilitate water infiltration, percolation, and aquifer replenishment under specific environmental and climatic conditions (Ouali et al., 2023), its thorough understanding and quantification are essential for the strategic management of the groundwater resources.

Based on this concept, groundwater recharge potential mapping (GWRPM) has been widely used to spatially delineate zones of varying groundwater availability through the integration of geospatial and statistical methods (Mosaad et al., 2026). To this end, several approaches have been applied to map groundwater recharge potential, including remote sensing (RS) techniques (Sunmin et al., 2020; Adams et al., 2022; Panday et al., 2023; Purdy et al., 2024), GIS (Varouchakis et al., 2022; Castañeda-Valbuena et al., 2023), machine learning (ML) and deep learning (DL) (Barzegar et al., 2024; Ali et al., 2024), as well as combined RS and ML approaches (Elmotawakkil et al.; Sadiki and Enneya, 2024). These methods were based on various statistical methodologies such as frequency ratio (Jayaraj et al., 2022), evidential belief function (Ghosh et al., 2021) and weight of evidence (Rane and Jayaraj, 2022). As well as several machine learning algorithms for the exploration of groundwater such as boosted regression tree (Prasad et al., 2020), random forest (Kumar et al., 2021; Masroor et al., 2021), artificial neural network (Nalivan et al., 2021), convolution neural network (Namous et al., 2021) and support vector machine (Prasad et al., 2020; Kumar et al., 2021). Despite the increasing use of RS-GIS and ML approaches for groundwater assessment, limited studies have focused on groundwater recharge potential in snow influenced semi-arid mountainous environments of Morocco, particularly under conditions of rapid agricultural expansion and climate variability.

In light of this research, we have employed several ML algorithms, such as random forest (RF), XGBoost (XGB) and frequency ratio (FR), to map the groundwater recharge potential zones, using measured piezometric observations, in the Midelt Aquifer region within the Ansegmir River watershed (ARW).

The ARW, set within a semi-arid continental climatic context, represents a first order water resource for the upper Moulouya basin; it feeds a network of 16 Saguia water intakes spanning over 300 km, and plays a pivotal role in local, regional, and national socio-economic development. Indeed, the ARW contributes more than 62,000 tons per year to the total apple production of Midelt province, which reached 370,000 tons in 2020 (Ouahi L., 2024).

The climatic conditions are particularly suited to apple tree cultivation, which represents the dominant agricultural activity in the ARW. However, apple orchards are highly water demanding crops, requiring from approximately 500 mm to 720 mm of water per growing season under semi-arid conditions in Morocco (El Jaouhari et al., 2018).To meet the water demands of apple orchard cultivation, farmers commonly rely on groundwater resources (Fuente-Saiz et al., 2024).

As a result, the Midelt aquifer faces significant challenges: climate change may progressively reduce groundwater recharge, while overexploitation through intensive agricultural pumping may cause a decline in piezometric levels and destabilize the hydrological cycle.

This assessment constitutes a prerequisite for evaluating groundwater recharge potential, establishing water budgets, developing hydrological and hydrogeological models, assessing groundwater quality, and implementing artificial recharge schemes through Managed Aquifer Recharge (MAR) approaches (El Farchouni et al., 2025).

Indeed, the present study, based on measured piezometric depth data, remote sensing (RS), GIS-based algorithms, and machine learning (ML) approaches, aims to map the groundwater recharge potential of the Midelt aquifer in response to orchard expansion within the ARW, particularly following the implementation of the Green Morocco Plan and the Generation Green Plan.

To achieve the specific objectives of this study, several factors considered to be the main controls influencing groundwater recharge potential were selected (Moumane et al., (2024); Agli et al., 2024), including hydroclimatic, topographic, geological, land use and vegetation factors, which were implemented and evaluated using three ML algorithms (RF, XGB and FR).The main contributions of this study are summarized as follows:

- To present, to the best of our knowledge, the first groundwater recharge potential map of the Oued Ansegmir Watershed (Upper Moulouya, Morocco) developed using directly measured piezometric observations from 271 drilling as the target variable;
- To integrate field measurements, in situ observations, remote sensing, GIS, and machine learning for groundwater recharge potential assessment in a snow influenced semi-arid mountain aquifer dominated by intensive apple orchards;
- To introduce a several levels of validation framework combining ten complementary performance metrics, inter-model agreement analysis based on Cohen's kappa coefficient, and pixel by pixel spatial validation using the spatial agreement score (SAS).

The resulting maps provide a decision support framework for sustainable groundwater management and future managed aquifer recharge planning in semi-arid watersheds of Morocco.

MATERIALS AND METHODS

Study area

Considered part of the Upper Moulouya Basin, the Oued Ansegmir Watershed (1060 km²) [Rahoui et al., 2024] constitutes the western extremity of the Meseta Oranaise. This watershed extends between the High Atlas to the south and the Middle Atlas to the north and northeast (Figure 1).

The climate of the ARW is characterized by low rainfall inputs with 396 mm/year, which is poorly distributed both in time and space (Rahoui et al., 2024). This distribution is subject to considerable intra and inter-annual variability, which can trigger intense storm events in the study area, particularly in the summer. Snowfall generally occurs above 1.500 m and persists only above 2.000 m on mountain peaks (Addou et al., 2023).

Over time, the geological evolution of the Ansegmir river watershed (Rahoui et al., 2024)

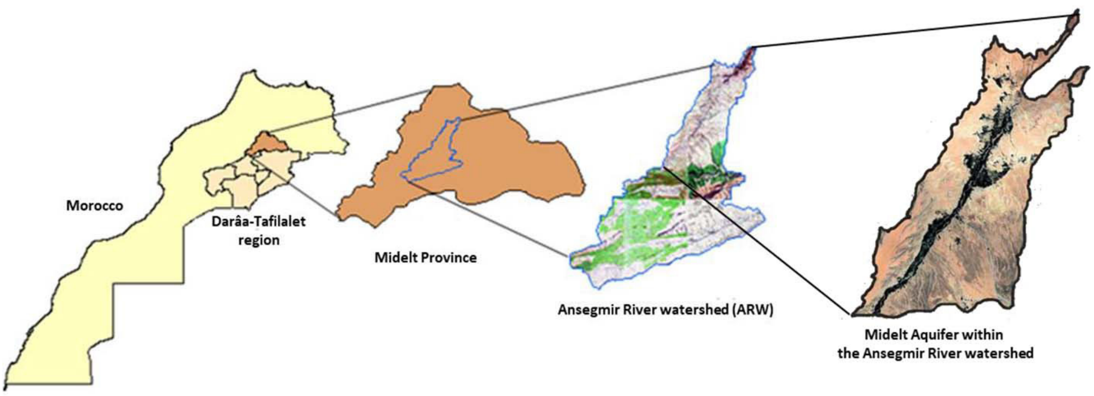

Figure 1. Location of the Midelt Aquifer within the Ansegmir River Watershed

led to the development of an aquifer known as the Midelt Aquifer (241.41 km²). This shallow, unconfined aquifer is primarily hosted within Miocene, Pliocene, and Quaternary formations, including conglomerates, alluvial deposits, and lacustrine limestones. (Ikhmerdi et al., 2018).

Data

In addition to the 271 piezometric measurements collected from boreholes during field investigations, piezometric depth data for the 2015-2020 period were obtained from the Moulouya Basin Agency of Midelt (Figure 2).

A total of 23 groundwater recharge conditioning factors were selected for groundwater recharge potential mapping, using measured piezometric observations, in the Midelt aquifer within the Oued Ansegmir watershed (ARW). Table 1 presents the conditioning factors, their corresponding Google Earth Engine (GEE) data sources, temporal filters, compositing, and the main GEE/QGIS processing steps.

All GEE derived layers were generated for the period, from 2015-01-01 to 2020-04-13, corresponding to the period of measured piezometric observations. MODIS products were converted to physical units by applying the appropriate scale factors (LST* 0.02; from Kelvin to °C, and ET*0.1), while Landsat 8 Collection 2 Level 2 surface reflectance bands were rescaled using a multiplicative factor of 0.0000275 and an additive offset of -0.2. Landsat images were masked for clouds and cloud shadows using the QA_PIXEL band and composited using the median reducer. All raster datasets were subsequently resampled to a common spatial resolution of 30 m and projected to the UTM Zone 30N coordinate system (EPSG:32630). Topographic derivatives, slope, aspect, curvature, topographic wetness index (TWI), and drainage density, were generated in QGIS 3.40.11 from the SRTM 1 Arc-Second DEM (USGS/SRTMGL1_003). In addition, inverse distance weighting (IDW) interpolation of precipitation data and Euclidean distance to waterways were computed in QGIS.

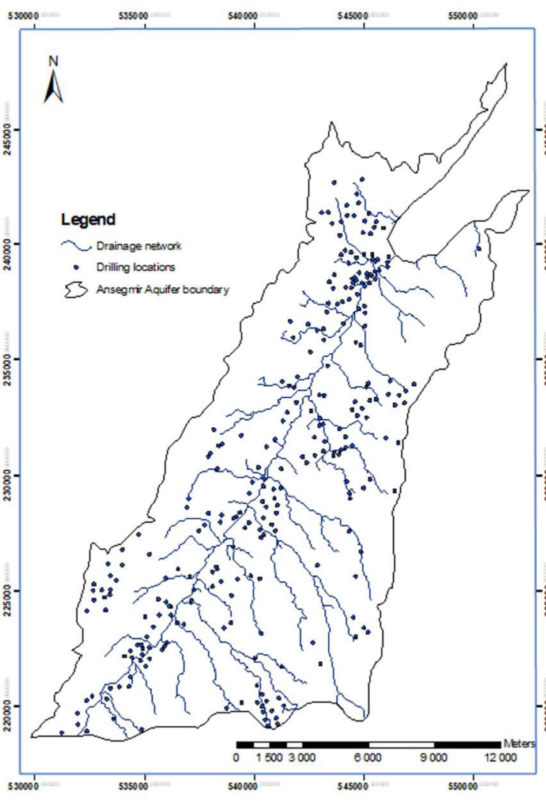

Figure 2. Drilling locations in the Midelt Aquifer

Methodological approach

The methodological approach adopted in this study was developed by building on previous groundwater studies conducted in Morocco, particularly those employing machine learning techniques (Table 2).

The proposed methodology integrates in situ field measurements (piezometric observations), remote sensing, GIS processing, machine learning, and spatial validation within a single workflow. Indeed, in the proposed research, the training and testing datasets were divided at a ratio of 70:30 for the development and validation of the ML model (Mosaad et al., 2026). The methodology consists of the following steps: The first step involves the acquisition of piezometric depth data with the corresponding spatial datasets collected in situ. The second step consists of preparing the various factors influencing groundwater. The third step is the generation of the training point matrix. The fourth step includes training and testing the used model. The fifth step involves validating and comparing the models used. Finally, the last step consists of mapping of the groundwater recharge potential using the selected algorithms (Figure 3).

All analyses were performed in the Python environment (Python 3.12.13) using the following packages: XGBoost 3.3.0, scikit-learn 1.6.1, pandas 2.2.2, NumPy 2.0.2, and SHAP 0.52.0.

Table 1. Data sources, formula and processing methods (GEE/QGIS workflow), and outputs of the conditioning factors used for groundwater recharge potential mapping, using measured piezometric observations, in the Midelt Aquifer region within the ARW

Factors	Indices	Data source	Formula / Processing method (QGIS & GEE)	Output
Climatic	P	Meteorological stations	Temporal aggregation and IDW interpolation in QGIS	Precipitation map
	ET	MODIS	Evapotranspiration extraction and temporal averaging in GEE	Evapotranspiration map
	LST	MODIS	Thermal band processing and emissivity correction in GEE	Land surface temperature map
Soil	Clay	FAO / SoilGrids	Spatial interpolation and raster resampling in QGIS	Clay content map
	Sand	FAO / SoilGrids	Spatial interpolation and raster resampling in QGIS	Sand content map
Lithologic and Geologic	FD	Extracted fractures from DEM and satellite imagery	Line density analysis in QGIS	Fracture density map
Topographic and Morphometric	DEM	SRTM DEM	DEM (digital elevation model) preprocessing in QGIS/GEE	Elevation map
	Slope	SRTM DEM	DEM preprocessing in QGIS	Terrain slope map
	Aspect	SRTM DEM	DEM preprocessing in QGIS	Slope orientation map
	Curvature	SRTM DEM	DEM derivative analysis in QGIS	Surface curvature map
	TWI	SRTM DEM	$TWI = \ln\left(\frac{As}{\tan\beta}\right)$ A_s: Specific area (total upslope area); *β:* Local slope angle.	Topographic wetness index map
Hydrological	DD	Extracted drainage network from DEM	$Dd = \frac{\sum L}{A}$ *ΣL:* Total length of drainage network; *A:* Area of the ARW.	Drainage density map
	DtW	Hydrographic network	Euclidean distance analysis in QGIS	Distance-to-waterways map
	MNDWI	Landsat imagery	$MNDWI = \frac{Green - SWIR}{Green + SWIR}$ *Green:* Green spectral band; *SWIR:* Short-Wave Infrared spectral band.	Modified normalized difference water index map
Vegetation	NDVI	Landsat imagery	$NDVI = \frac{NIR - Red}{NIR + Red}$ *NIR:* Near Infrared spectral band; *RED:* Red spectral band.	Normalized difference vegetation index map
	GNDVI	Landsat imagery	$GNDVI = \frac{NIR - Green}{NIR + Green}$	Green normalized difference vegetation index map
	SAVI	Landsat imagery	$SAVI = \frac{(NIR - Red)(1 + L)}{NIR + Red + L}$ *L :* Calibration constant (commonly 0.5).	Soil adjusted vegetation index map
	NDFI	Landsat imagery	Spectral fraction analysis in GEE	Normalized difference fraction index map
Land Use	LULC	Landsat imagery	Land use classification in QGIS	Land use land cover map
	LU	Landsat imagery	Supervised classification (RF/SVM) in GEE	Land use map
	BSI	Landsat imagery	$BI = \frac{(SWIR + Red) - (NIR + Blue)}{(SWIR + Red) + (NIR + Blue)}$ *Blue:* Blue spectral band.	Bare soil index map
	BU	Landsat imagery	Combination of built-up indices in GEE	Built-up area map
	NDBI	Landsat imagery	$NDBI = \frac{SWIR - NIR}{SWIR + NIR}$	Normalized difference built-up index map

RESULTS

Data collection

Unlike most groundwater recharge potential studies that rely on expert defined or inventory based labels (Karimi et al., 2021). This study uses field measured piezometric depths from 271 boreholes as the target variable. The Empirical Bayesian Kriging (EBK) method was then applied to estimate the spatial distribution of groundwater levels across the Midelt aquifer

Table 2. Comparison of the present study with previous Moroccan studies

Study	Data	Models	Validation	Novelty
Namous et al. (2021)	Twenty-four groundwater influencing factors; 374 groundwater springs inventoried	Random Forest, logistic regression, decision tree and artificial neural networks	Curve (ROC) method and compound factor (CF) method	Groundwater potentiality mapping in mountainous aquifers, Essaouira, Morocco
Ouali et al. (2023)	Twenty three GWP influencing factors and 884 binary data	Multilayer perceptron, k-nearest neighbor, decision tree, and support vector machine algorithms, voting, random forest, adaptive boosting, gradient boosting, extreme gradient boosting and the deep learning neural network	Average area	Groundwater potential mapping in an oasis area, Morocco
Marchane et al. (2023)	Fracture networks; Hercynian orogeny	Box-counting method	Fractal dimension (FD)	Potentiality of groundwater recharge in the region of Smaâla, Morocco
Elmotawakkil et Al. (2024)	GWP influencing factors	Gradient boosting regression, support vector regression, Random Forest and decision tree	R^2, Mean Absolute Error and Root Mean Squared Error	Predicting groundwater level, Rabat-Kénitra region, Morocco.
Moumane et al. (2024)	Key factors influencing recharge	Weighted linear combination	AUC/ROC	Mapping groundwater recharge potential zones, Kenitra, Morocco
El Farchouni et al. (2025)	Six recharge factors	Analytical hierarchy process and stable isotopes	Stable isotopes (δ18O and δ2H)	Mapping groundwater recharge potential zones, Tensift basin, Morocco
The present study	Twenty three influencing indices and measured piezometric depths from 271 boreholes	Random forest, XGBoost, and frequency ratio	Ten complementary metrics, Cohen's kappa coefficient and Spatial Agreement Score	Groundwater recharge potential mapping in the ARW, Morocco

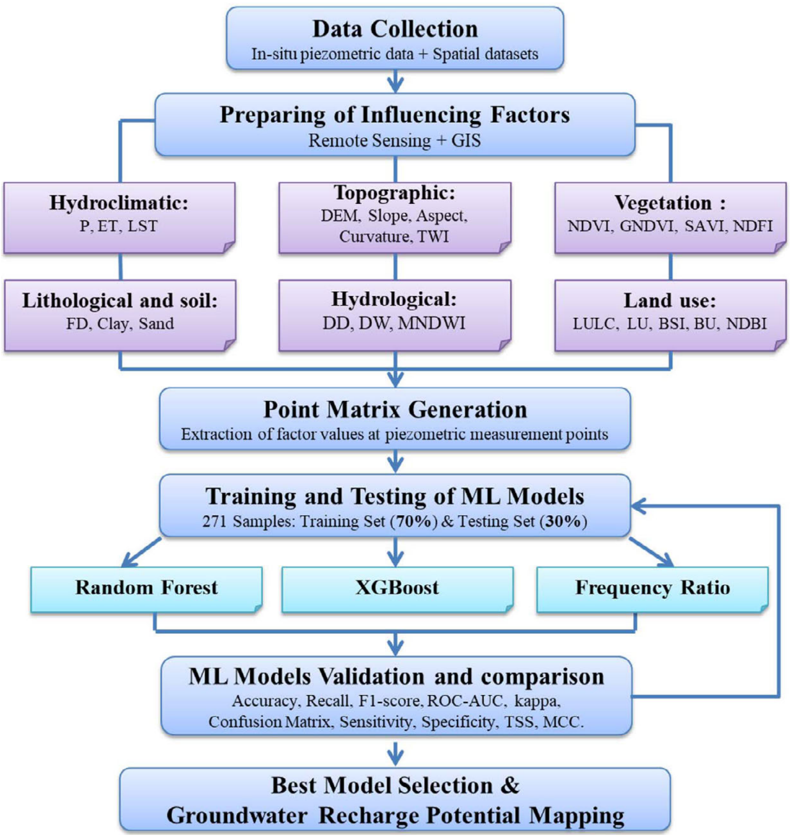

Figure 3. Flowchart of the methodology

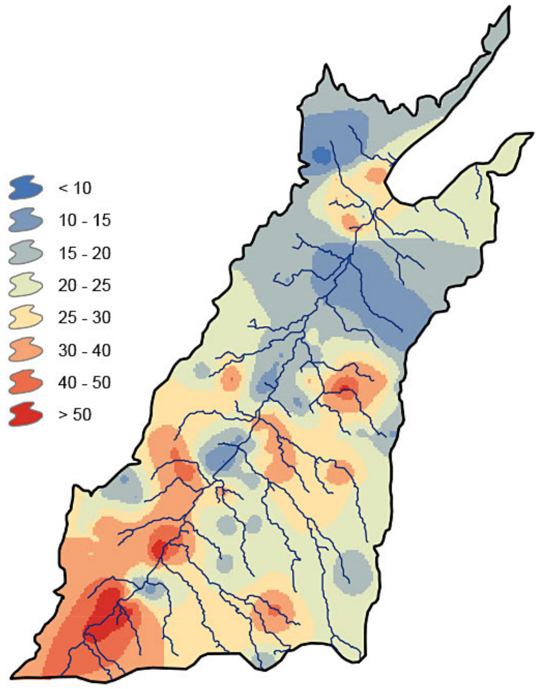

Figure 4. Groundwater depth map (m) (Piezo)

within the Oued Ansegmir watershed (Figure 4), providing an observation driven ground truth for ML models development.

Preparing of influencing factors

The potentiality of groundwater is directly related to climatic factors (Bera, 2020). Notably, precipitation (P), evapotranspiration (ET), land surface temperature (LST) in the Midelt Aquifer region within the ARW (Figure 5).

The soil type factor can be considered a major influencing factor (Mukhopadhyay, 2020). The recharge of the Midelt Aquifer, through rainfall infiltration, depends on the properties of the different soil types, mainly CLAY and SAND (Figure 6). Fracture density (FD) is considered one of the most important lithologic and geologic factors influencing groundwater recharge and flow (Mukesh et al., 2023) (Figure 7).

The groundwater potential is closely related to topographic and morphometric factors (Biswas et al., 2020). The recharge of the Midelt Aquifer depends on the elevation (DEM), terrain slope (SLOPE), slope orientation (Aspect), surface curvature (Curvature) and topographic wetness index (TWI) (Figure 8).

In this research, the hydrological factors are represented by drainage density (DD), distance to waterways (DW), and the modified normalized difference water index (MNDWI) (Pinto et al., 2017) (Figure 9). The vegetation factors are represented by the normalized difference vegetation index (NDVI), Green normalized difference vegetation index (GNDVI), soil adjusted vegetation index (SAVI), and normalized difference fraction index (NDFI) (Prasad et al., 2020) (Figure 10).

The recharge of the Midelt Aquifer also depends on land use, mainly represented by land use/land cover (LULC), bare soil index (BSI), built-up areas (BU), and the normalized difference built-up index (NDBI) (Biswas et al., 2020) (Figure 11).

Generation of the training point matrix

To generate the point matrix, the values of the factors controlling the groundwater recharge potential of the Midelt Aquifer within

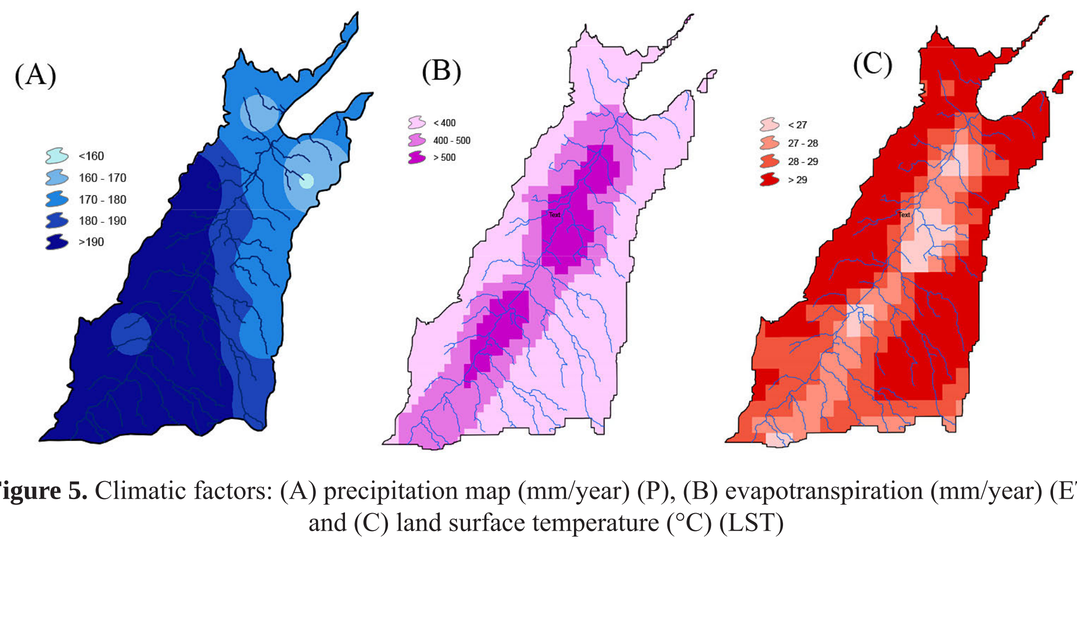

Figure 5. Climatic factors: (A) precipitation map (mm/year) (P), (B) evapotranspiration (mm/year) (ET), and (C) land surface temperature (°C) (LST)

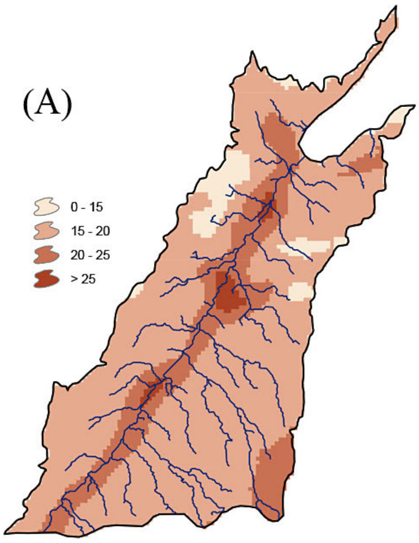

Figure 6. Soil type factors: (A) clay and (B) sand

the ARW were extracted at each sampling point. A total of 271 piezometric samples were used to extract the values of 23 groundwater recharge conditioning factors. The resulting database was organized into a point matrix and subsequently used for statistical analysis and model development.

Based on the Pearson correlation matrix calculated using 23 explanatory variables to assess multicollinearity. A threshold of $r \geq 0.8$ (Dormann et al., 2013) was used to identify pairs of highly collinear variables; in each pair, the variable that

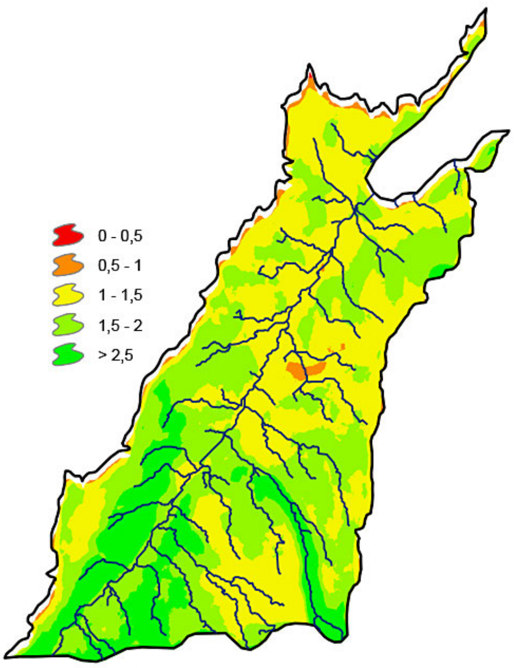

Figure 7. Geologic factor – fracture density (FD)

was least physically relevant or most redundant was subsequently excluded from the analyses.

In fact, the Pearson correlation matrix reveals several pairs of variables with perfect or near perfect correlations, indicating redundancy in the data. For the first group of variables with a redundancy links the spectral indices NDFI and NDBI (r=-1.000) due to their mathematically opposite formulations.

A second group of variables with strong correlations (r ranging from 0.93 to 0.997) includes, on the one hand, vegetation indices, NDVI, SAVI, and GNDVI with r values between +0.98 and +0.997, all of which measure the vigor of plant biomass, and on the other hand, bare soil and built up area indices, BSI, BU, and NDBI with r values between +0.93 and +0.99, which characterize bare and impervious surfaces. These two groups are also strongly negatively correlated with each other (for example, NDVI and BSI with r = -0.95; NDVI and BU with r = -0.87), reflecting the natural opposition between vegetation cover and bare soil. Moderate correlations are also observed with the following variables: P and DEM (r = +0.74); MNDWI and NDVI (r = -0.78); and DD and DtW (r = -0.66).

It is also observed that the piezometric variable (Piezo) exhibits weak linear correlations with all explanatory factors, with $r < 0.17$, which justifies the use of nonlinear models such as Random Forest (RF), XGBoost (XGB) and Frequency Ratio (FR).

Based on this analysis, seven variables were removed to reduce multicollinearity, namely:

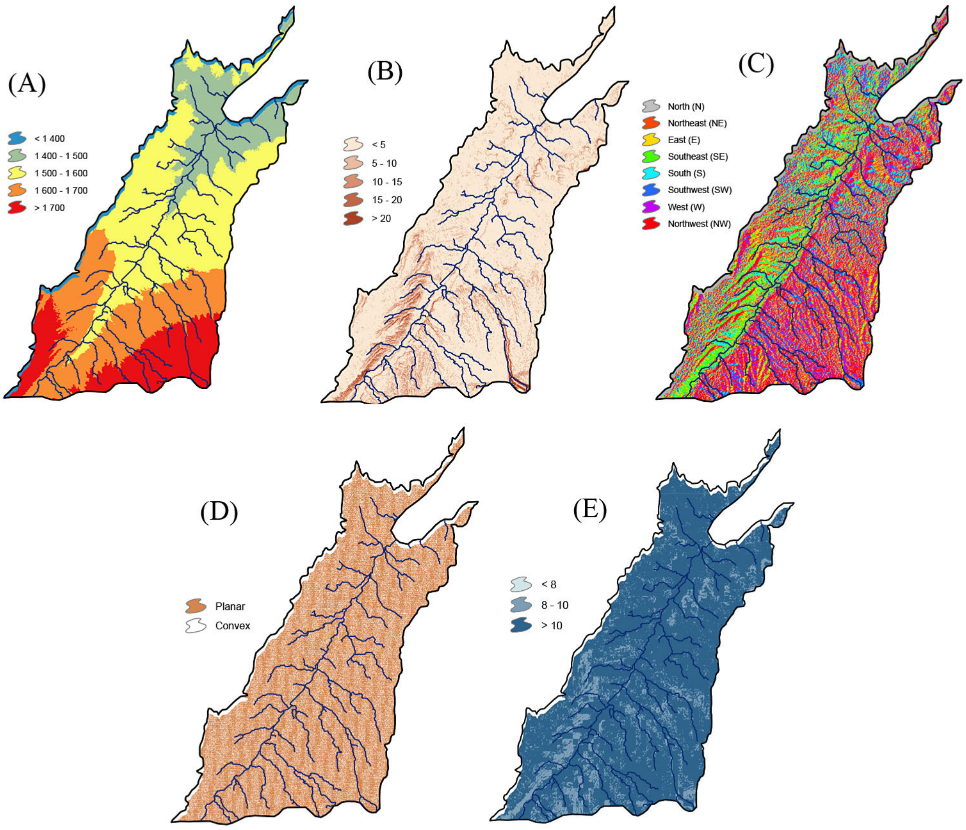

Figure 8. Topographic and morphometric factors: (A) elevation (m) (DEM), (B) SLOPE (%), (C) slope orientation (ASPECT), (D) CURVATURE and (E) topographic wetness index (TWI)

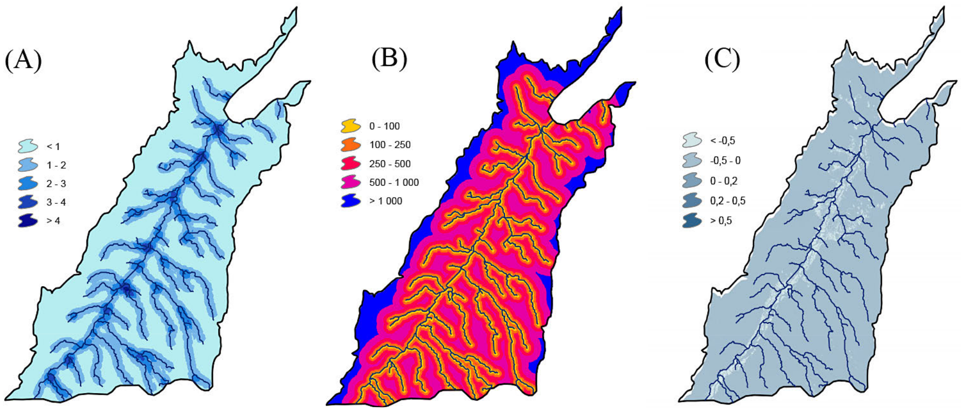

Figure 9. Hydrological factors: (A) drainage density (km/km^2) (DD), (B) distance to waterways (m) (DtW) and (C) modified normalized difference water index (MNDWI)

CURVATURE (redundant with FD), NDFI and NDBI (perfectly anticorrelated), SAVI and GNDVI (redundant with NDVI), as well as BU and BSI (redundant with NDVI via the vegetation-bare soil axis) (Figure 12).

To confirm the absence of residual multicollinearity after removing redundant variables using Pearson's correlation, variance inflation factors (VIFs) (Dormann et al., 2013; O'Brien, 2007) were calculated for the 16 selected explanatory variables (n = 271). All VIFs are less than 5 (NDVI: 4.14; DEM: 3.79; MNDWI: 3.55; the others are less than 3). (Figure 13).

All 16 explanatory variables have variance inflation factors (VIF) below 5, confirming the absence of residual multicollinearity.

In this study, the variable (Piezo) representing the piezometric depth was converted into a binary target variable: 1 = high recharge potential (<20 m) and 0 = low recharge potential

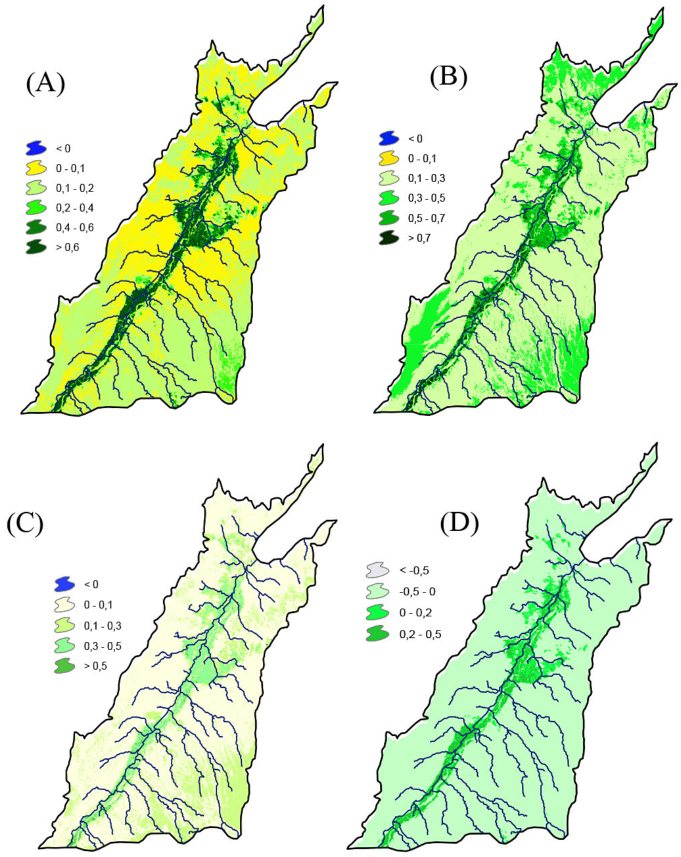

Figure 10. Vegetation factors: (A) normalized difference vegetation index (NDVI), (B) green normalized difference vegetation index (GNDVI), (C) soil adjusted vegetation index (SAVI) and (D) normalized difference fraction index (NDFI)

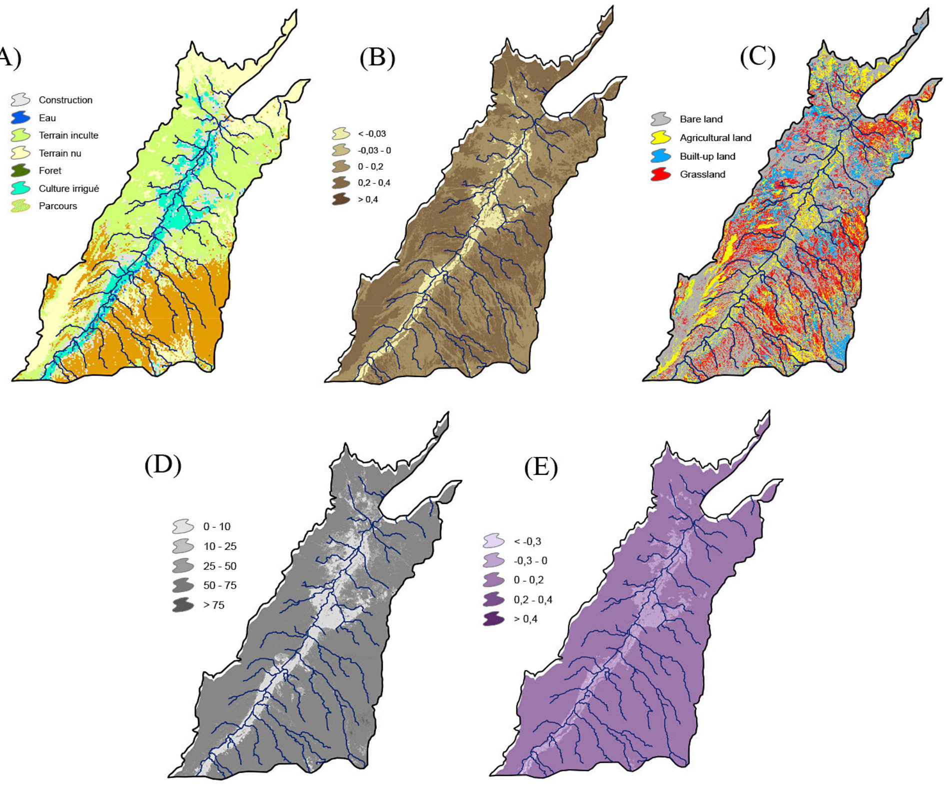

Figure 11. Land use factors: (A) land use/land cover (LULC), (B) bare soil index (BSI), (C) land use (LU), (D) built-up areas (BU) and (E) normalized difference built-up index (NDBI)

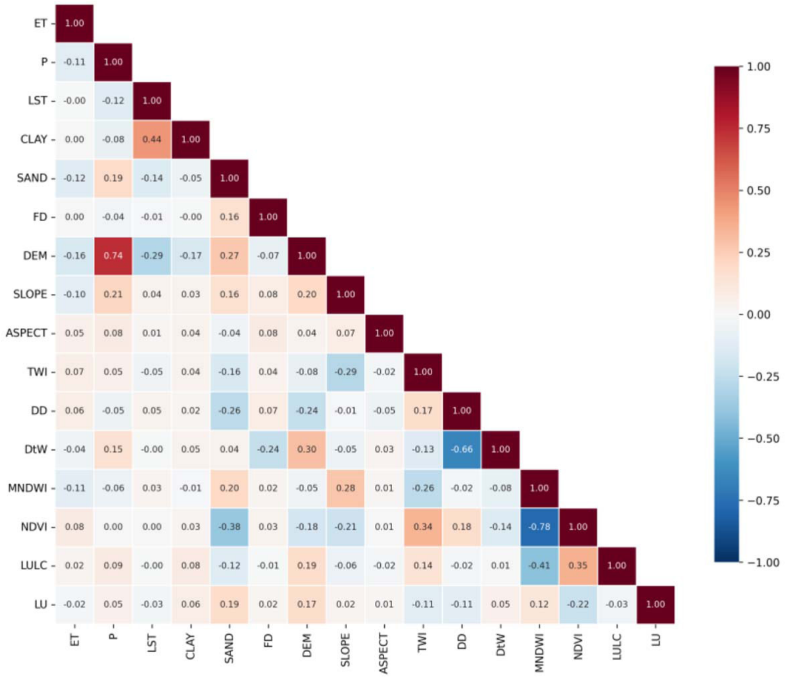

Figure 12. Pearson correlation matrix (lower triangle) for 16 factors controlling the groundwater recharge potential of the Midelt Aquifer

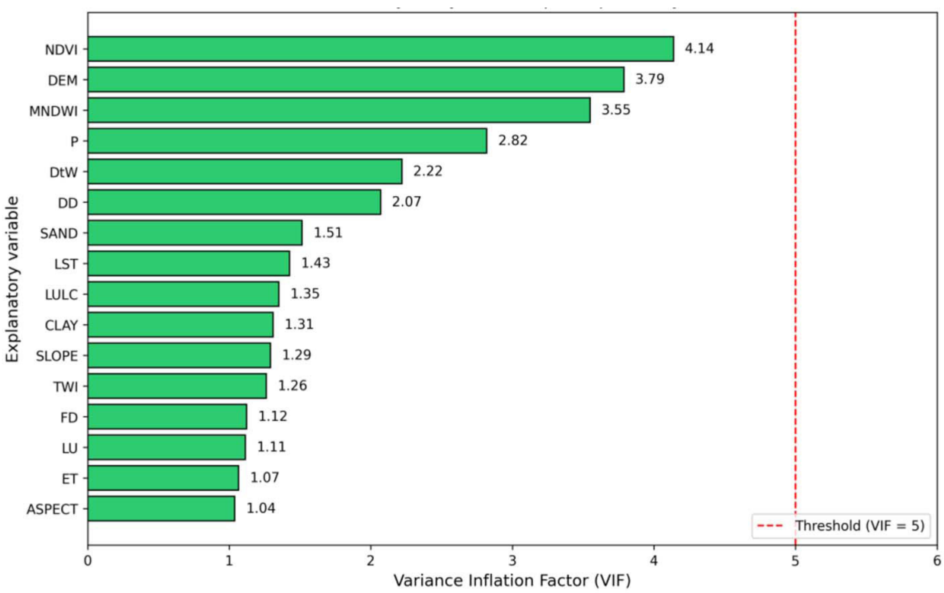

Figure 13. Variance inflation factor (VIF) plot for multicollinearity analysis of 16 factors controlling the groundwater recharge potential of the Midelt Aquifer

(≥20 m), given that 20 m is the median of the 271 measured depths, as this formulation allows for the use of standard threshold-based performance metrics, such as the area under the ROC curve (AUC), which has become the benchmark for comparing machine learning models in groundwater recharge potential mapping (Naghibi et al., 2017; Arabameri et al., 2019).

Training and testing the used model

The dataset (n=271) was randomly divided (random_state=42) into a training subset (70%, n=190) and a test subset (30%, n=82), using stratified sampling to preserve class proportions. The hyperparameters of the RF, XGB and FR classifiers were optimized using grid search combined with 10 fold stratified cross validation on the training subset, using the area under the ROC curve (AUC) as the objective metric. The optimized models were then evaluated on the independent test subset, which had been set aside throughout the optimization procedure (Naghibi et al., 2017).

Frequency ratio

The frequency ratio (FR) is a simple and transparent bivariate statistical method that quantifies the relationship between each conditioning factor and groundwater recharge potential. Owing to its interpretability and widespread application in groundwater potential mapping, it serves as an appropriate baseline model for comparison. The FR model estimates the contribution of each conditioning factor by comparing the percentage of points to the percentage of pixels (Das et al., 2019) (Figure 14):

$$FR = \frac{\%\,points}{\%\,pixels} \tag{1}$$

By summing the frequency ratio values, using the matrix calculation function, for each factor influencing groundwater recharge potential (GWRP), the groundwater recharge potential index (GWRPI) was derived (Kumar et al. 2023).

$$\begin{aligned} GWRPI = {} & ET_{FR} + P_{FR} + LST_{FR} + CLAY_{FR} + \\ & + SAND_{FR} + FD_{FR} + DEM_{FR} + SLOPE_{FR} + \\ & + ASPECT_{FR} + TWI_{FR} + DD_{FR} + DtW_{FR} + \\ & + MNDWI_{FR} + NDVI_{FR} + LULC_{FR} + LU_{FR} \end{aligned} \tag{2}$$

The continuous map of the GWRPI index reveals a marked gradient across the Midelt aquifer (Figure 15.B). Indeed, the ranking of variable contributions derived from the Frequency Ratio model (Figure 15.A) identifies precipitation (P), fracture density (FD), elevation (DEM), and evapotranspiration (ET) as the four dominant predictors of groundwater recharge potential in the Midelt aquifer.

In contrast, the ASPECT and TWI variables have the lowest contributions. The remaining factors, however, have a moderate influence

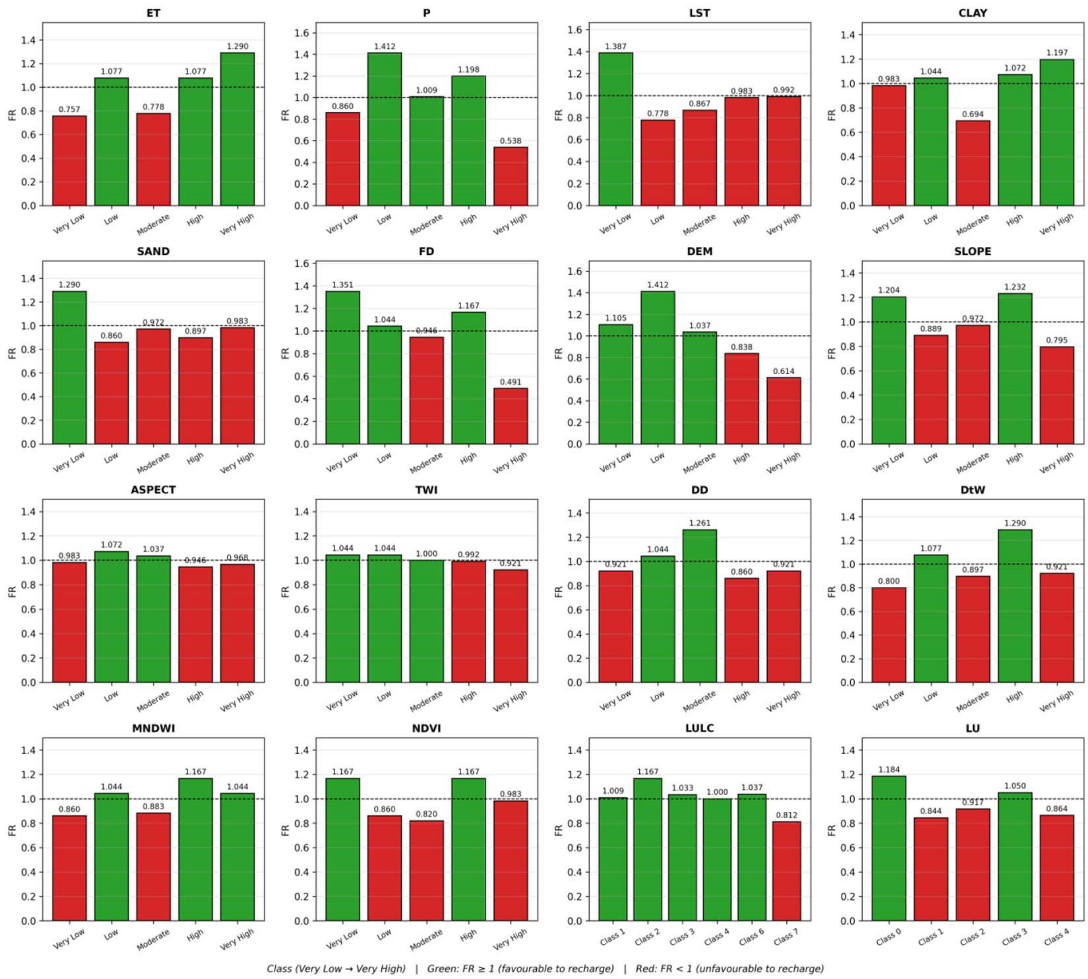

Figure 14. Frequency ratio values per class and per explanatory factor (n = 16 variables)

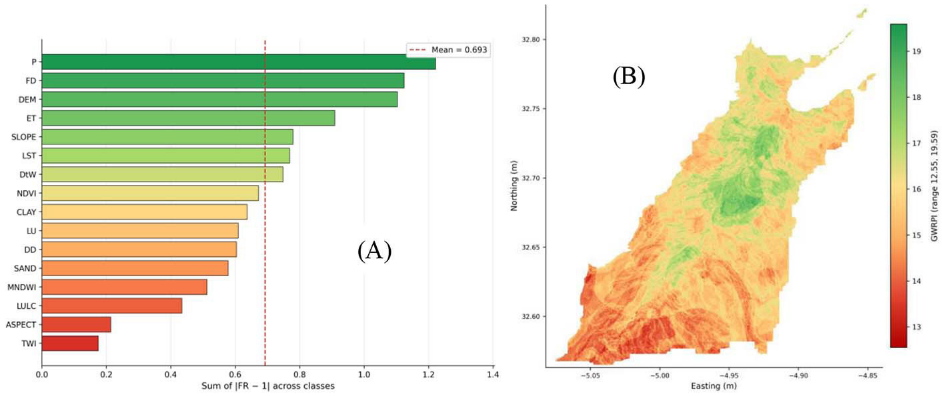

Figure 15. (A) Variable contribution and (B) continuous groundwater recharge potential index (GWRPI) derived from the Frequency Ratio model

on the spatial distribution of recharge within the FR model.

Random forest

Random forest (RF) was selected because it can effectively capture complex non-linear relationships, and interactions among groundwater recharge potential conditioning factors. Its bagging based ensemble strategy improves model robustness by reducing variance and limiting overfitting. While its ability to handle heterogeneous predictor variables without feature scaling makes it well suited to the diverse environmental datasets used in this study.

The final prediction is obtained by aggregating the predictions of all individual trees through majority voting (Singh et al., 2023). Following hyperparameter optimization, the RF model was configured with n_estimators: 100, max_depth: None, max_features: ‘sqrt’, and min_samples_split: 2.

The probability distribution (Figure 16) has a quasi Gaussian shape, centered around 0.40 and extending broadly across the entire interval [0, 0.9], which indicates good probabilistic calibration of the random forest model. The predicted mean probability is slightly below the decision threshold of 0.5; We note that 67.0% of the study area is classified as having low potential (Class 0, water table > 20 m) and 33.0% as having high potential (Class 1, water table < 20 m), which indicates a moderate overall recharge potential at the scale of the Midelt aquifer (Figure 17).

The ranking of variables by importance derived from the random forest model (Figure 18.A) indicates that elevation (DEM), precipitation (P), fracture density (FD), and evapotranspiration (ET) are the most influential predictors of groundwater recharge potential in the Midelt aquifer. In contrast, land use (LULC) and land cover (LU) have the lowest importance values. Variables related to soil texture, particularly clay and sand content, as well as soil surface temperature (LST), also contribute significantly to the model. As for the other factors, they make a moderate contribution to the spatial prediction of groundwater recharge potential.

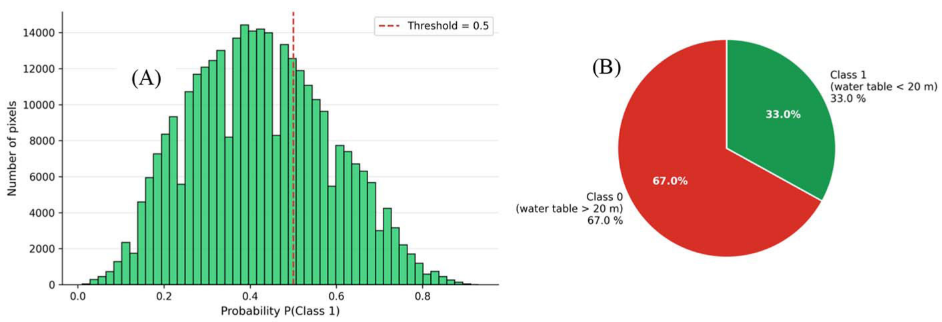

Figure 16. Distribution of predicted probabilities using the RF model: (A) probability histogram and (B) spatial distribution of classes

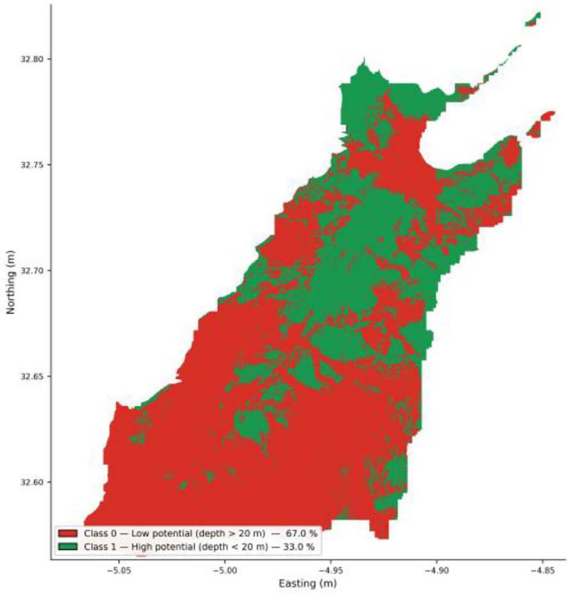

Figure 17. Binary classification map generated using the RF model

The SHAP analysis of the random forest model (Figure 18.B) confirms the feature importance ranking; elevation (DEM), fracture density (FD), precipitation (P), and evapotranspiration (ET) are identified as the most influential predictors, whereas LU, LULC, drainage density (DD), slope (SLOPE), and slope aspect (ASPECT) contribute the least to the model predictions. Beyond ranking, the SHAP summary plot reveals both the magnitude and direction of each contribution of features to groundwater recharge potential. Positive SHAP values increase the predicted recharge potential, whereas negative SHAP values reduce it. The color scale represents feature values, with red indicating high values and blue indicating low values, showing that the influence of each feature varies according to its value.

Overall, the SHAP results suggest that elevation, fracture density, precipitation, and evapotranspiration are the main contributors to the RF model predictions of groundwater recharge potential.

Extreme gradient boosting

Extreme gradient boosting (XGBoost) is a boosting based ensemble learning algorithm that sequentially improves predictive performance by correcting the errors of previously generated trees. Its built in regularization mechanisms and efficient tree optimization enhance model generalization and make it well suited for tabular geospatial datasets and moderate sample sizes. At each boosting iteration, a new decision tree is constructed to minimize the residual errors of the existing ensemble using gradient descent optimization. The final prediction is obtained by combining the contributions of all trees in the ensemble (Chen and Guestrin, 2016). Following hyperparameter optimization, the XGBoost model was configured with n_estimators = 100, max_depth = 5, learning_rate = 0.01, subsample = 1.0, gamma: 0.1, and colsample_bytree = 0.8.

The probability distribution is bimodal (Figure 19), with a first peak around 0.28–0.32 and a second, more pronounced peak around 0.44–0.48, as well as a tail extending toward higher probabilities (up to 0.72). The predicted average probability is below the decision threshold of 0.5; We find that 72.2% of the study area is classified as having low potential (Class 0, water

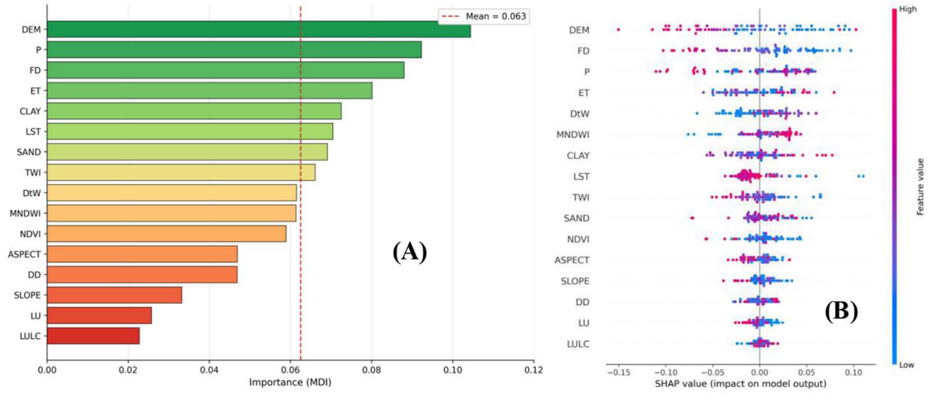

Figure 18. Groundwater recharge potential factors importance using the RF model: (A) feature importance ranking and (B) SHAP summary plot (Beeswarm)

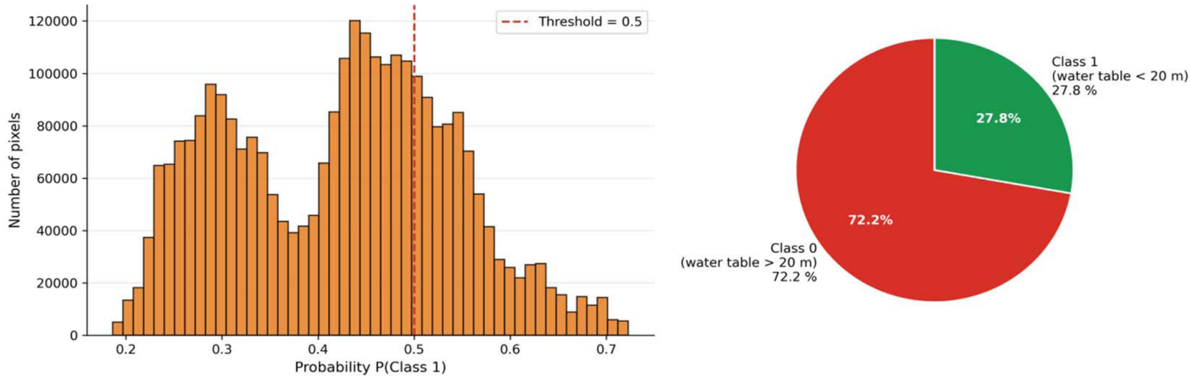

Figure 19. Distribution of predicted probabilities using the XGB model: (A) probability histogram and (B) spatial distribution of classes

table > 20 m) and 27.8% as having high potential (Class 1, water table < 20 m), indicating a moderate to low overall recharge potential at the scale of the Midelt aquifer (Figure 20).

The ranking of variables by importance, based on the XGBoost model (Figure 21.A), indicates that evapotranspiration (ET), precipitation (P), elevation (DEM), flow direction (FD), and clay content (CLAY) are the most influential predictors of groundwater recharge potential in the Midelt aquifer. Conversely, LU, slope aspect (ASPECT), and LULC have the lowest importance values. As for the other factors, they make a moderate contribution to the spatial prediction of groundwater recharge potential in the Midelt aquifer.

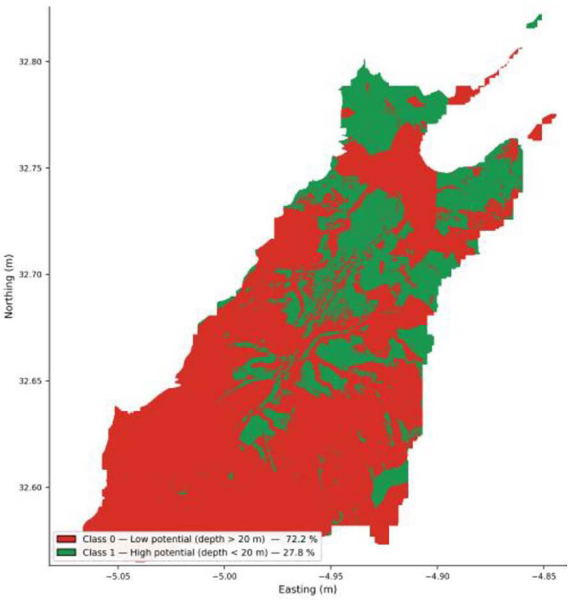

Figure 20. Binary classification map generated using the XGB model

The SHAP analysis of the XGBoost model (Figure 21.B) confirms the feature importance ranking; P, DEM, CLAY, ET and FD represent the most influential predictors, while LU, ASPECT, and LULC contribute the least.

These results provide additional insight into the XGBoost model and its application to groundwater recharge potential mapping in the Midelt aquifer.

DISCUSSION

ML models validation and comparison

To perform a comparative validation and evaluate the predictive performance of the three algorithms used for groundwater recharge potential mapping, using measured piezometric observations, in the Midelt aquifer (Random Forest, XGBoost, and frequency ratio), model performance was assessed using an independent test dataset (n=82). The evaluation was carried out through ROC curves, confusion matrices, radar charts, multi-metric bar plots, and a validation heatmap; Ten model validation metrics were computed, namely: Area under the ROC curve (AUC), accuracy, balanced accuracy, sensitivity, specificity, true skill statistic (TSS), precision, F1-score, Cohen's kappa coefficient, and Matthews correlation coefficient (MCC). Inter-model agreement was further assessed using pairwise Cohen's Kappa coefficients between model predictions and pixel-by-pixel spatial agreement among the generated groundwater recharge potential maps. Finally, the best-performing model was identified based on a composite performance score and was subsequently selected to

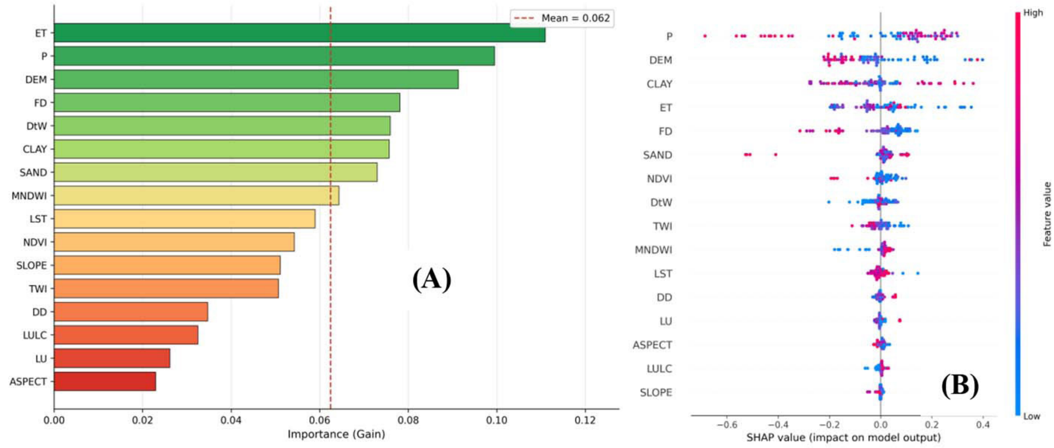

Figure 21. Groundwater recharge potential factors importance using the XGBoost model: (A) feature importance ranking and (B) SHAP summary plot (Beeswarm)

produce the final groundwater recharge potential map of the Midelt aquifer.

The comparative ROC curves and confusion matrices on the test set (Figure 22) reveal that XGBoost achieves the highest discriminative power with an AUC of 0.769, followed by Random Forest (AUC = 0.752), while the Frequency Ratio model lags behind (AUC = 0.649).

XGBoost correctly classified 39 of the 47 low recharge samples (true negatives) and 18 of the 35 high recharge samples (true positives), achieving a Cohen's kappa of 0.356. Random Forest classified 36 true negatives and 20 true positives, with a Cohen's Kappa of 0.342, reflecting a slightly higher recall for the minority class. The frequency ratio model, with only 29 true negatives and 17 true positives, with a Cohen's kappa of 0.103, confirms its weaker classification skill compared with the XGB and RF algorithms.

To evaluate these models, ten performance metrics computed for each model (Figure 23). XGBoost outperforms the other two models on the majority of indicators; AUC (0.769), accuracy (0.695), balanced accuracy (0.672), specificity (0.830), TSS (0.344), precision (0.692), Kappa (0.356) and MCC (0.366). Random Forest, however, achieves the highest sensitivity (0.571) and F1-score (0.606), indicating a more balanced detection of recharge favourable zones but with a lower precision. The frequency ratio model ranks third across all metrics, with particularly low TSS, Kappa and MCC values (all = 0.103).

According to the box plot of the scores (Figure 24), the Random Forest model gives the clearest class separation; median scores of 0.370 vs. 0.550 for low and high recharge and a spread of 0.180. While the XGBoost model

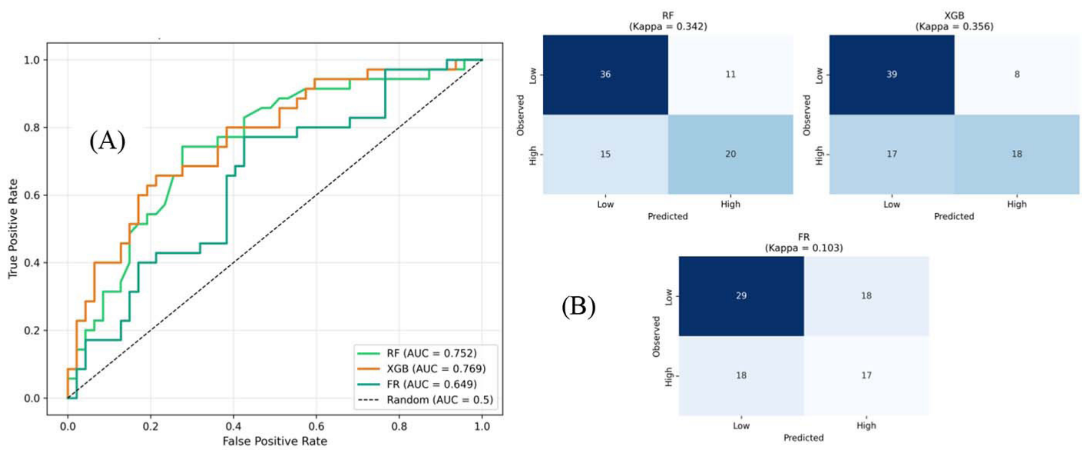

Figure 22. Discrimination power and classification accuracy: (A) comparative ROC curves and (B) confusion matrices of the three retained models on the independent test set (n = 82)

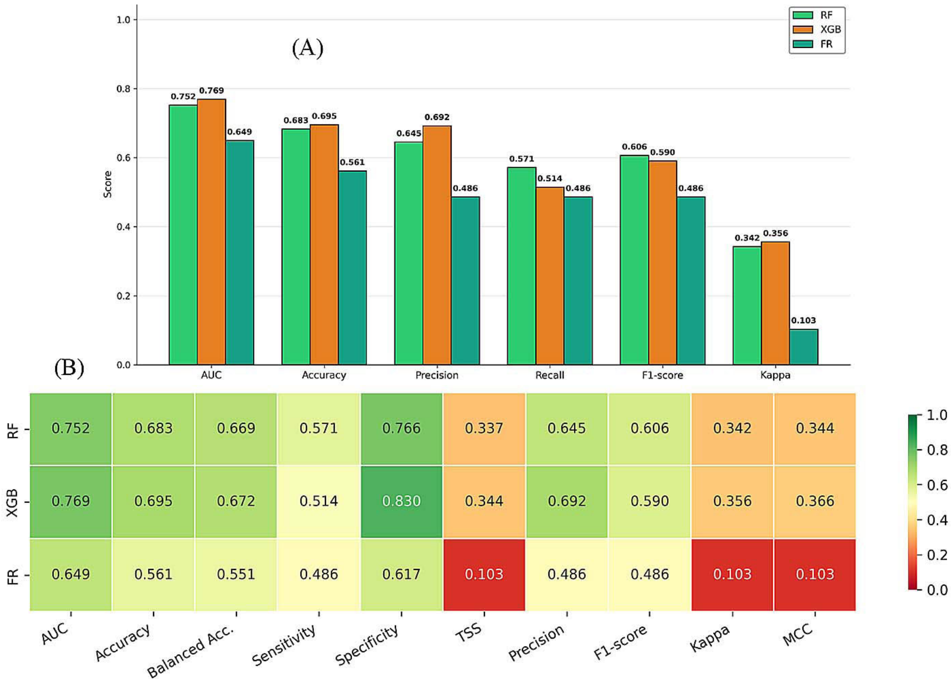

Figure 23. (A) Bar chart and (B) extended validation heatmap of ten (10) performance metrics computed on the independent test set (n = 82)

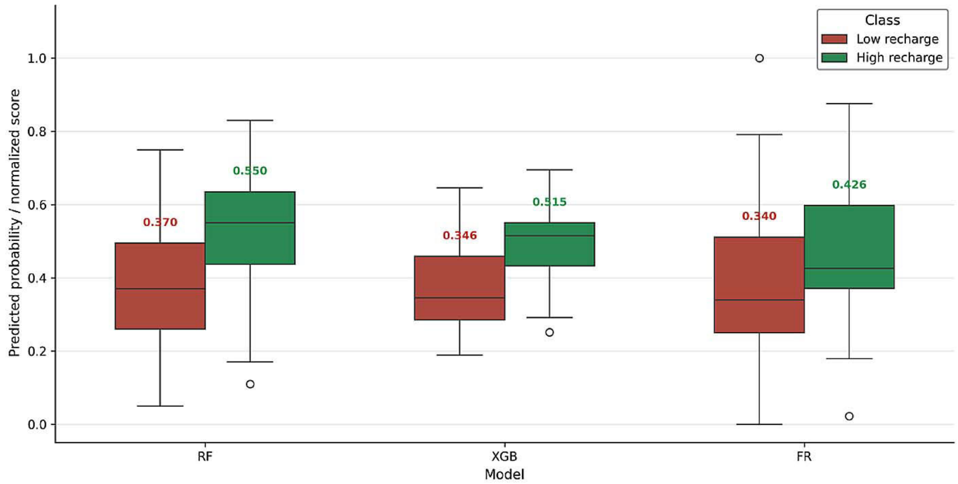

Figure 24. Boxplot of predicted scores per observed class

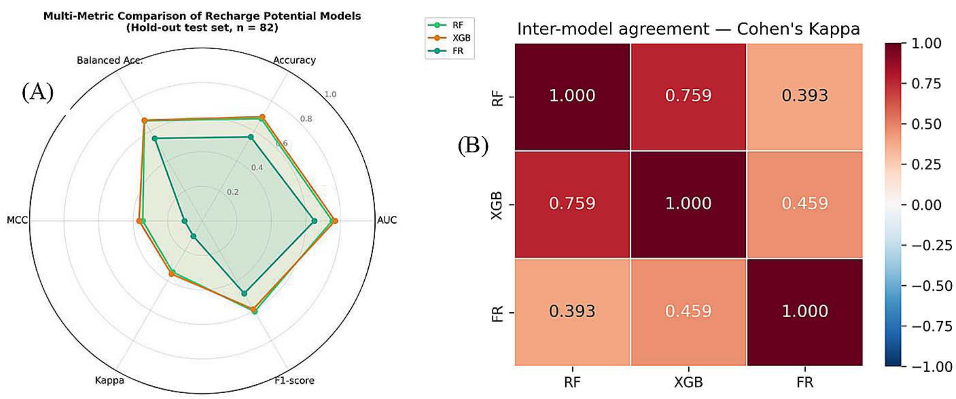

Figure 25. (A) Radar chart and (B) pairwise Cohen's Kappa matrix between model predictions

gives median scores of 0.346 versus 0.515 for low and high recharge and a spread of 0.169. In contrast, the FR model shows a significantly smaller deviation of only 0.086 and gives median scores of 0.340 compared to 0.426 for low and high recharge. This reflects the limited ability of bivariate methods to capture multivariate nonlinear interactions between the 16 conditioning factors.

The radar polygons (Figure 25. A) of RF and XGBoost virtually overlap and extend toward the outer rings of the chart, while the FR polygon is significantly smaller, especially along the Kappa and MCC axes. In contrast, the pairwise Cohen's Kappa matrix between model predictions (Figure 25.B) reveals substantial agreement between RF and XGBoost models (Kappa = 0.759), confirming that the two ensemble algorithms produce highly consistent classifications. In comparison, the FR model shows moderate agreement with both machine learning models (Kappa = 0.393 with RF and 0.459 with XGB).

The spatial distribution of the five classes of recharge potential over the 241.41 km² of the Midelt aquifer at the ARW (Table 3) reveals notable differences among the models. The XGBoost model assigns 54.1% (130.6 km²) of the study area to the 'Moderate' recharge potential class, while allocating only 0.6 km² to the 'Very Low' class and no area to the 'Very High' class. In contrast, the Random Forest model produces a more differentiated distribution, with 18.6 km², 36.8 km², and 2.0 km² classified as 'Very low', 'High', and 'Very High' recharge potential class, respectively. The Frequency Ratio map, generated through quantile-based reclassification, partitions the study area equally among the five classes, with approximately 48.3 km² per class by construction (Figure 26).

To validate the spatial distribution presented above, a spatial validation was performed by overlaying the 82 independent test points (30% holdout dataset) on the groundwater recharge potential maps produced by the three models selected (Figure 27).

Table 3. Surface distribution of the five recharge potential classes (km² and percentage) for each model on the Midelt aquifer

Parameter	FR		RF		XGB	
	S (km²)	%	S (km²)	%	S (km²)	%
Very Low	48.28	20.0	18.61	7.7	0.57	0.2
Low	48.28	20.0	90.08	37.4	94.96	39.3
Moderate	48.28	20.0	93.74	38.9	130.64	54.1
High	48.28	20.0	36.76	15.2	15.24	6.3
Very High	48.28	20.0	2.23	0.8	0.00	0.0
TOTAL	241.41	100.0	241.41	100.0	241.41	100.0

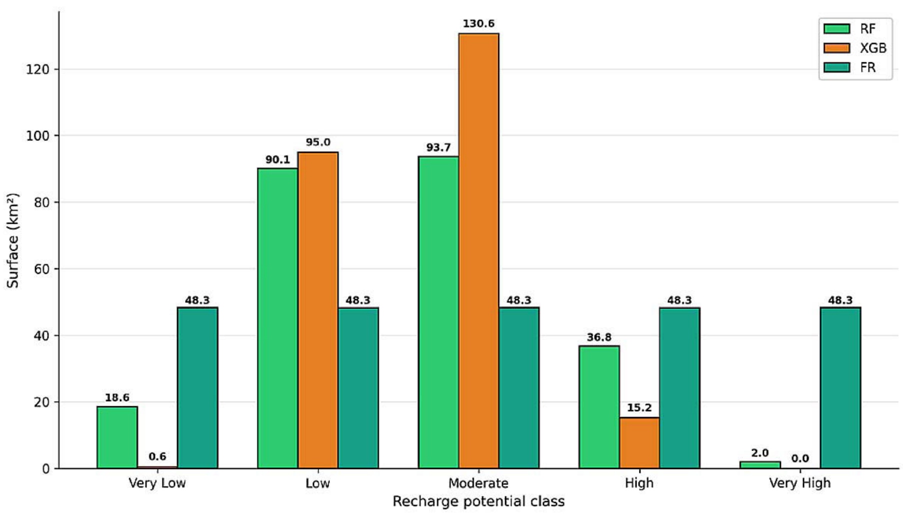

Figure 26. Surface distribution by recharge potential class and model

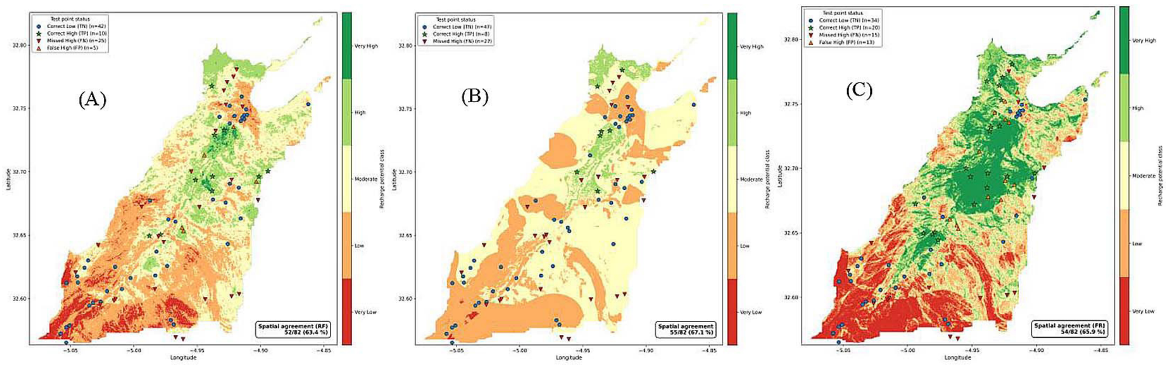

Figure 27. Groundwater recharge potential maps produced by the three models selected: (A) RF map, (B) XGB map and (C) FR map

Each test point was classified into one of four prediction categories, namely: true negatives (TN), representing observed and predicted low recharge; true positives (TP) representing high and predicted high recharge; false negatives (FN) corresponding to observed high recharge incorrectly predicted as low recharge; and false positives (FP) corresponding to observed low recharge incorrectly predicted as high recharge. The spatial agreement score (SAS), defined as the proportion of correctly classified points (TN + TP)/n, provides an explicit geographical complement to the confusion matrix based performance metrics presented above.

The spatial validation highlighted a notable characteristic of the map produced by XGBoost; The highest spatial agreement score (SAS=69.5%) with the strongest specificity for the low recharge class, 39 true negatives out of 47 and only 8 false positives, while still correctly identifying a substantial proportion of high groundwater recharge potential areas, 18 true positives out of 35. The Random Forest model achieved the highest detection rate for the high recharge class, 20 true positives out of 35, but at the expense of 11 false positives, which lowered its specificity with spatial agreement score (SAS=68.3). The Frequency Ratio model, through its reclassification by equal area quantiles, identified 17 true positives out of 35 but produced the largest number of false positives (18) and the lowest spatial agreement score (SAS = 56.1%) (Table 4).

Best model selection and groundwater recharge potential mapping

Based on both the spatial distribution of the predicted recharge potential and a composite performance score integrating AUC, F1 score, Cohen's Kappa and MCC, the XGBoost model was identified as the best performing model and was selected to generate the final groundwater recharge potential map of the Midelt aquifer (Figure 28).

The selected XGBoost map highlights two main groups of favorable recharge zones, located primarily in the central part and the Northwestern parts of the Midelt aquifer within ARW, whereas the Southern and Southwestern margins are dominated by low and very low recharge potential classes.

This spatial prediction is consistent with the hydrogeological context of the region (Rahoui et Al., 2024), where groundwater recharge is primarily controlled, according to the XGB model, by climatic factors (ET and P), the topographic factor (DEM), geological and lithological factors (FD), the hydrological factor (DtW) and pedological factors (Clay and Sand), which act as preferential infiltration zones.

Table 4. Summary of the spatial agreemen of the RF, XGB and FR models

Model	TN	TP	FN	FP	SAS (%)
RF	36	20	15	11	68.3
XGB	39	18	17	8	**69.5**
FR	29	17	18	18	56.1

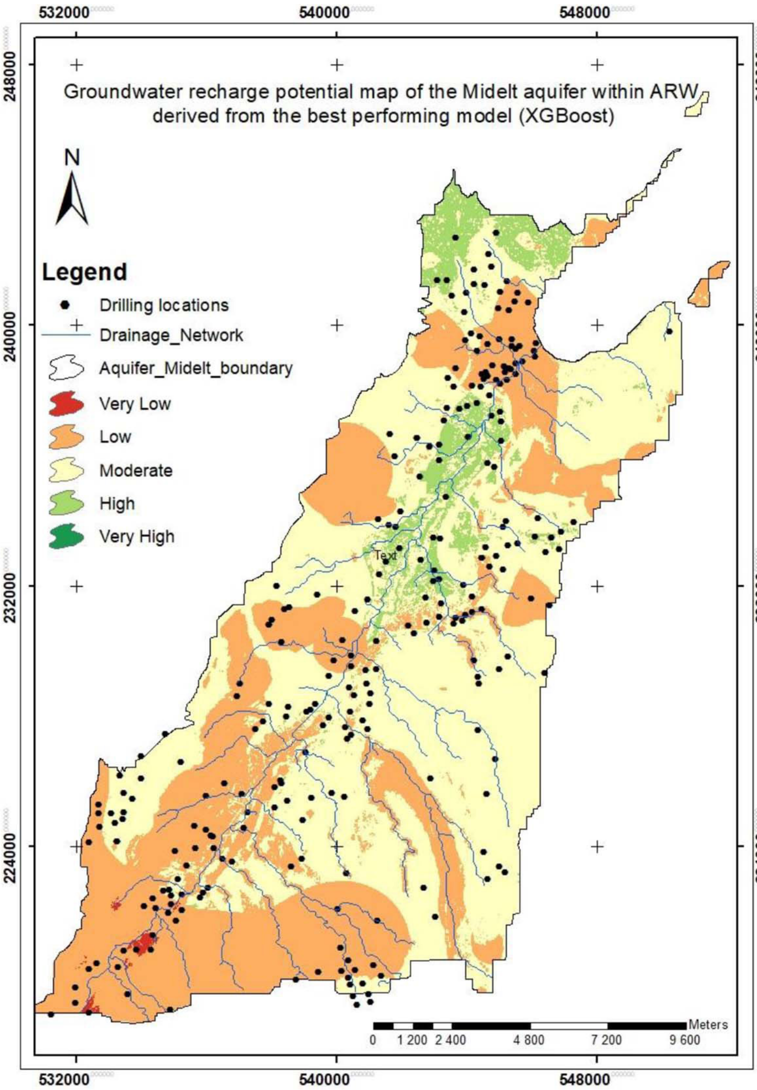

Figure 28. Final groundwater recharge potential map of the Midelt aquifer derived from the best-performing model (XGBoost)

CONCLUSIONS

To map the groundwater recharge potential of the Midelt aquifer (241 km²), in response to the expansion of orchards within the Oued Ansegmir watershed, This study integrated piezometric data, remote sensing (RS), GIS-based algorithms and ML approaches. Three modeling techniques were compared: FR, RF and XGBoost; using 271 measured piezometric observations divided into training (70%) and testing (30%) datasets and 23 initial conditioning factors.

Following the acquisition of piezometric data and preparation of potential recharge conditioning factors, a training matrix was generated for the calibration and validation of the three models. After multicollinearity analysis using the Pearson correlation matrix and the variance inflation factor (VIF), 16 conditioning factors were retained for modeling.

The performances of the FR, XGB and RF models were evaluated using ten validation metrics, namely: area under the ROC curve (AUC), accuracy, balanced accuracy, sensitivity, specificity, true skill statistic (TSS), precision, F1-score, Cohen's kappa coefficient, and Matthews correlation coefficient (MCC); In addition, spatial validation was performed by overlaying the 82 independent test points on the groundwater recharge potential maps produced by the three models.

Among the evaluated algorithms, XGBoost demonstrated the best predictive performance and was selected to generate the final groundwater recharge potential map of the Midelt aquifer at the ARW. The XGB model achieved an AUC of 0.769, an F1 of 0.590, and a Cohen's kappa of 0.356. The resulting map highlights that low recharge areas, mainly located in the southern and southwestern margins of the aquifer, were identified with perfect specificity (47 true negatives out of 47 and no false positive). Conversely, high recharge areas, predominantly in the central and in the northwestern part of aquifer, were identified with caution (8 true positives out of 35).

These results provide a scientific basis, grounded in field measured data, for the sustainable management of groundwater resources and for the prioritizing future drilling investments in the downstream part of the Oued Ansegmir watershed. Further investigations integrating geophysical field surveys are recommended to refine the transitional zones identified by the XGBoost model and to improve the delineation of groundwater recharge potential.

REFERENCES

1. Acharki, S., Boudhar, A., Bouihrouchane, A., Bousbaa, M., Karaoui, I., Elyoussfi, H., Bargam, B., El Khalki, E.M., Hadri, A., Chehbouni, A. (2025). Spatial modeling of snow water equivalent in the High Atlas Mountains via a lumped process-based approach. *Scientific Reports, 15*, 26327. https://doi.org/10.1038/s41598-025-12163-8
2. Adams, E.A., et al. (2022). Remote sensing of groundwater: Current capabilities and future directions. *Water Resources Research.* https://doi.org/10.1029/2022WR032219
3. Addou, R., Hanchane, M., Krakauer, N.Y., Kessabi, R., Obda, K., Souab, M., Achir, I.E. (2023). Wavelet analysis for studying rainfall variability and regionalizing data: An applied study of the Moulouya watershed in Morocco. *Applied Sciences, 13*(6), 3841. https://doi.org/10.3390/app13063841
4. Agli, S., et al. (2024). Delineation of groundwater storage and recharge potential zones using multi-influencing factors (MIF) method: Application in synclinal coastal basin of Essaouira (Western High Atlas of Morocco). *Geomatics and Environmental Engineering.* https://doi.org/10.7494/geom.2024.18.4.117
5. Ali, M., et al. (2024). An overview of deep learning applications in groundwater level modeling. *Applied Computational Intelligence and Soft Computing*. https://doi.org/10.1155/2024/9480522
6. Arabameri, et al. (2019). Application of probabilistic and machine learning models for groundwater potentiality mapping in Damghan sedimentary plain, Iran. *Remote Sensing, 11*(24), 3015. https://doi.org/10.3390/rs11243015
7. Barzegar, R., Jafarzadeh, F., Moghaddam, A.A., Razzagh, S., Cloutier, V., Rosa, E. (2024). A meta-ensemble machine learning strategy to assess groundwater holistic vulnerability in coastal aquifers. *Groundwater for Sustainable Development, 26*, 101296. https://doi.org/10.1016/j.gsd.2024.101296
8. Bera, A., Mukhopadhyay, B.P., Barua, S. (2020). Delineation of groundwater potential zones in Karha river basin, Maharashtra, India, using AHP and geospatial techniques. *Arabian Journal of Geosciences, 13*, 693. https://doi.org/10.1007/s12517-020-05702-2
9. Biswas, S., Mukhopadhyay, B.P., Bera, A. (2020). Delineating groundwater potential zones of agriculture dominated landscapes using GIS based AHP techniques: a case study from Uttar Dinajpur district, West Bengal Uttar Dinajpur, *Environmental Earth Sciences, 79*(12). https://doi.org/10.1007/s12665-020-09053-9
10. Boudhar, A., Hanich, L., Boulet, G., Duchemin, B., Berjamy, B., Chehbouni, A. (2009). Evaluation of the snowmelt Runoff Model in the Moroccan High Atlas Mountains using two snow-cover estimates. *Hydrological Sciences Journal, 54*(6), 1094–1113. https://doi.org/10.1623/hysj.54.6.1094
11. Boudhar, A., Ouatiki, H., Bouamri, H., Lebrini, Y., Karaoui, I., Hssaisoune, M., Arioua, A., Benabdelouahab, T. (2020). *Hydrological response to snow cover changes using remote sensing over the Oum Er Rbia Upstream Basin, Morocco.* In: Mapping and Spatial Analysis of Socio-Economic and Environmental Indicators for Sustainable Development (pp. 95–102). Springer. https://doi.org/10.1007/978-3-030-21166-0_9
12. Castaneda-Valbuena, D., et al. (2023). Assessment of changes in regional groundwater levels through spatio-temporal kriging: Application to the southern basin of Mexico. *Hydrogeology Journal.* https://doi.org/10.1007/s10040-023-02681-y
13. Das, S. (2019). Comparison among influencing factor, frequency ratio, and analytical hierarchy process techniques for groundwater potential zonation in Vaitarna Basin, Maharashtra, India. *Groundwater for Sustainable Development, 8*, 617–629. https://doi.org/10.1016/j.gsd.2019.03.003
14. Döll, P., Flörke, M. (2005). *Global-scale estimation of diffuse groundwater recharge: Model Tuning to Local Data for Semi-Arid and Arid Regions and Assessment of Climate Change Impact.* Frankfurt Hydrology Paper No. 03, Institute of Physical Geography, Frankfurt University, Frankfurt am Main, Germany.
15. Dormann, C.F., Elith, J., Bacher, S., Buchmann, C., Carl, G., Carré, G., Marquéz, J.R.G., Gruber, B., Lafourcade, B., Leitão, P.J., Münkemüller, T., McClean, C., Osborne, P.E., Reineking, B., Schröder, B., Skidmore, A.K., Zurell, D., Lautenbach, S.

(2013). Collinearity: a review of methods to deal with it and a simulation study evaluating their performance. *Ecography, 36*(1), 27–46. https://doi.org/10.1111/j.1600-0587.2012.07348.x

16. El Farchouni, A., Hadri, A., Fakir, Y., Ouarani, M., Azaroual, M., Kchikach, A. (2025). Mapping groundwater recharge potential zones in a semi-arid, anthropogenically modified mountainous basin. *Scientific African, 30*, e03025. https://doi.org/10.1016/j.sciaf.2025.e03025
17. El Jaouhari, N., Abouabdillah, A., Bouabid, R., Bourioug, M., Aleya, L., Chaoui, M. (2018). Assessment of sustainable deficit irrigation in a Moroccan apple orchard as a climate change adaptation strategy. *Science of the Total Environment, 642*, 574–581. https://doi.org/10.1016/j.scitotenv.2018.06.108
18. Elmotawakkil, A., Sadiki, A., Enneya, N. (2024). Predicting groundwater level based on remote sensing and machine learning: A case study in the Rabat-Kenitra region. *Journal of Hydroinformatics, 26*(10), 2639–2667. https://doi.org/10.2166/hydro.2024.494
19. Fuente-Saiz, D., Ortega-Farias, S., Carrasco-Benavides, M., Ortega-Salazar, S., Tian, F., Wang, S., Liu, Y. (2024). Assessment of satellite-based water requirements for a drip-irrigated apple orchard in Mediterranean agroclimatic conditions. *Heliyon, 10*(9), e29688. https://doi.org/10.1016/j.heliyon.2024.e29688
20. Ghosh, B. (2021). Spatial mapping of groundwater potential using data-driven evidential belief function, knowledge-based analytic hierarchy process and an ensemble approach. *Environmental Earth Sciences, 80*(18), 625. https://doi.org/10.1007/s12665-021-09921-y
21. Hanich, L., Chehbouni, A., Gascoin, S., Boudhar, A., Jarlan, L., Tramblay, Y., Boulet, G., Marchane, A., Baba, M.W., Kinnard, C., Simonneaux, V., Fakir, Y., Bouchaou, L., Leblanc, M., Le Page, M., Bouamri, H., Er-Raki, S., Khabba, S. (2022). Snow hydrology in the Moroccan Atlas Mountains. *Journal of Hydrology: Regional Studies, 42*, 101101. https://doi.org/10.1016/j.ejrh.2022.101101
22. Ikhmerdi, H., Boukdir, A., Kossir, A., Alili, L., Ben-Said, E. (2018). Hydrogeological functioning of the tablecloth of the Midelt Furrow (High Moulouya, Morocco). *E3S Web of Conferences, 37*, 01002. https://doi.org/10.1051/e3sconf/20183701002
23. Jasechko, S., Perrone, D. (2021). Global groundwater wells at risk of running dry. *Science, 372*(6540), 418-421. https://doi.org/10.1126/science.abc2755
24. Karimi. R.S., Valipoori G. H., Hatami A. J. (2021). Groundwater-potential mapping using a self-learning Bayesian Network Model: A comparison among metaheuristic algorithms, *Water, 13*(5), 658;https://doi.org/10.3390/w13050658
25. Kumar, R., Dwivedi, S.B., Gaur, S. (2021). A comparative study of machine learning and Fuzzy-AHP technique to groundwater potential mapping in the data-scarce region. *Computers & Geosciences, 155*, 104855. https://doi.org/10.1016/j.cageo.2021.104855
26. Kumar, M., Singh, P., Singh, P. (2023). Machine learning and GIS-RS-based algorithms for mapping the groundwater potentiality in the Bundelkhand region, India. *Ecological Informatics, 74*, 101980. https://doi.org/10.1016/j.ecoinf.2023.101980
27. Leduc, C., Favreau, G., Schroeter, P. (2001). Long-term rise in a Sahelian water-table: The continental terminal in South-West Niger. *Journal of Hydrology, 243*(1–2), 43–54. https://doi.org/10.1016/S0022-1694(00)00403-0
28. Lee, S., et al. (2020). Groundwater potential mapping using remote sensing and GIS-based machine learning techniques. *Remote Sensing, 12*(7), 1200. https://doi.org/10.3390/rs12071200 (cite « Sunmin L. et al., 2020 » dans le texte)
29. Marchane, A., et al. (2023). Mapping of potential groundwater recharge sites in the Smaâla area (Central Morocco). *Journal of African Earth Sciences, 200*, 104888. https://doi.org/10.1016/j.jafrearsci.2023.104888
30. Masroor, M., Sajjad, H., Rahaman, M.H., Sahana, M., Ahmed, R., Singh, R. (2021). Assessing the impact of drought conditions on groundwater potential in Godavari Middle Sub-Basin, India using analytical hierarchy process and random forest machine learning algorithm. *Groundwater for Sustainable Development, 13*, 100554. https://doi.org/10.1016/j.gsd.2021.100554
31. Meng, F., Khan, M.I., Naqvi, S.A.A., Sarwar, A., Islam, F., Ali, M., Tariq, A., Ullah, S., Soufan, W., Faraj, T.K. (2024). Identification and mapping of groundwater recharge zones using multi influencing factor and analytical hierarchy process. *Scientific Reports, 14*, 19240. https://doi.org/10.1038/s41598-024-70324-7
32. Mosaad, M.A.H., Elsadek, E.A., Williams, C., Thorp, K.R., Elshikha, D.E.M. (2026). Groundwater potential mapping using machine learning techniques: Current trends and future perspectives. *Water, 18*(8), 947. https://doi.org/10.3390/w18080947
33. Moumane, A., et al. (2024). Integrating GIS, remote sensing, and analytic hierarchy process (AHP) for mapping of groundwater-recharge potential zones in Kenitra Province, Morocco: Toward sustainable development goals achievement. *Euro-Mediterranean Journal for Environmental Integration.* https://doi.org/10.1007/s41207-024-00706-w
34. Mukhopadhyay, B.P., Biswas, S., Bera, A. (2020). Delineating groundwater potential zones of agriculture dominated landscapes using GIS based

AHP techniques: A case study from Uttar Dinajpur district, West Bengal. *Environmental Earth Sciences, 79*, 302. https://doi.org/10.1007/s12665-020-09053-9

35. Naghibi, S.A., Ahmadi, K., Daneshi, A. (2017). Application of support vector machine, random forest, and genetic algorithm optimized Random Forest models in groundwater potential mapping. *Water Resources Management, 31*(9), 2761–2775. https://doi.org/10.1007/s11269-017-1660-3
36. Nalivan, O.A., Chowdhuri, I., Saha, A., Lee, S., Moayedi, H. (2021). Modeling groundwater potential using novel GIS-based machine-learning ensemble techniques. *Journal of Hydrology: Regional Studies, 36*, 100848. https://doi.org/10.1016/j.ejrh.2021.100848
37. O'Brien, R.M. (2007). A caution regarding rules of thumb for variance inflation factors. *Quality & Quantity, 41*(5), 673-690. https://doi.org/10.1007/s11135-006-9018-6
38. Ouahi, L., Ait Hou, M., Camanzi, L., Prosperi, P., Amin, R. (2024). Attitudes and preferences of the Moroccan consumer towards fruits: The case of the Midelt apple (Morocco). *The Economics & Management Review,* (2).
39. Ouali, L., Kabiri, L., Namous, M., Hssaisoune, M., et al. (2023). Spatial prediction of groundwater withdrawal potential using shallow, hybrid, and deep learning algorithms in the Toudgha Oasis, Southeast Morocco. *Sustainability, 15*(5), 3874. https://doi.org/10.3390/su15053874.
40. Pande, C.B., Moharir, K.N. (2021). *Groundwater resources development and planning in the semi-arid region*. Springer. https://doi.org/10.1007/978-3-030-68124-1
41. Panday, D.P., et al. (2023). Application of remote sensing techniques to deal with scale aspects of GRACE data to quantify groundwater levels. *MethodsX*. https://doi.org/10.1016/j.mex.2023.102108
42. Pinto, D., Shrestha, S., Babel, M.S., Ninsawat, S. (2017). Delineation of groundwater potential zones in the Comoro watershed, Timor Leste using GIS, remote sensing and analytic hierarchy process (AHP) technique. *Applied Water Science, 7*(1), 503–519. https://doi.org/10.1007/s13201-015-0270-6
43. Namous, M., Hssaisoune, M., Lee, C.-W., Alamri, A., Elaloui, A., Edahbi, M., Krimissa, S., Eloudi, H., Ouayah, M., et al. (2021). Spatial prediction of groundwater potentiality in large semi-arid and karstic mountainous region using machine learning models. *Water, 13*(16), 2273. https://doi.org/10.3390/w13162273
44. Prasad, P., Loveson, V.J., Kotha, M., Yadav, R. (2020). Application of machine learning techniques in groundwater potential mapping along the west coast of India. *GIScience & Remote Sensing, 57*(6), 735–752. https://doi.org/10.1080/15481603.2020.1794104
45. Purdy, A.J., et al. (2024). *Groundwater monitoring with GRACE.* In Cloud-based remote sensing with Google Earth Engine. Springer. https://doi.org/10.1007/978-3-031-26588-4_40
46. Rahoui, H., et al. (2024). Impact of climate conditions on the water potential of the River Ansegmir Watershed (Morocco). *Ecological Engineering & Environmental Technology, 25*(10), 107–117. https://doi.org/10.12912/27197050/191362
47. Rane, N.L., Jayaraj, G.K. (2022). Comparison of multi-influence factor, weight of evidence and frequency ratio techniques to evaluate groundwater potential zones of basaltic aquifer systems. *Environment, Development and Sustainability, 24*(2), 2315–2344. https://doi.org/10.1007/s10668-021-01535-5
48. Scanlon, B.R., Keese, K.E., Flint, A.L., Flint, L.E., Gaye, C.B., Edmunds, W.M., Simmers, I. (2006). Global synthesis of groundwater recharge in semiarid and arid regions. *Hydrological Processes, 20*(15), 3335–3370. https://doi.org/10.1002/hyp.6335
49. Singh, P., Kumar, M., Singh, P. (2023). Machine learning and GIS-RS-based algorithms for mapping the groundwater potentiality in the Bundelkhand region, India. *Ecological Informatics, 74*, 101980. https://doi.org/10.1016/j.ecoinf.2023.101980
50. Varouchakis, E.A., et al. (2022). Spatiotemporal geostatistical analysis of groundwater level in aquifer systems of complex hydrogeology. *Water Resources Research, 58*(3). https://doi.org/10.1029/2021WR029988
51. Fuente-Saiz, D., et al. (2024). Assessment of satellite-based water requirements for a drip-irrigated apple orchard in Mediterranean agroclimatic conditions. *Heliyon, 10*(9), e29688. https://doi.org/10.1016/j.heliyon.2024.e29688